ISA Transactions 151 (2024) 51–61

Contents lists available at ScienceDirect

ISA Transactions

journal homepage: www.elsevier.com/locate/isatrans

Research article

Sliding mode observer-based model predictive tracking control for Mecanum-wheeled mobile robot

Dongliang Wang [a,b], Yong Gao [c,d], Wu Wei [c,d,*], Qiuda Yu [c,d], Yuhai Wei [c,d], Wenji Li [a,b], Zhun Fan [e]

[a] School of Department of Electronic and Information Engineering, Shantou University, 515063, Guangdong, China
[b] Key Lab of Digital Signal and Image Processing of Guangdong Province, Shantou University, 515063, Guangdong, China
[c] School of Automation Science and Engineering, South China University of Technology, Guangzhou 510641, Guangdong, China
[d] Key Laboratory of Autonomous Systems and Networked Control, Ministry of Education, Guangzhou, 510640, Guangdong, China
[e] Shenzhen Institute for Advanced Study, University of Electronic Science and Technology of China, 518038, Guangdong, China

ARTICLE INFO

Keywords:
Mecanum-wheeled mobile robot
Model predictive control
Sliding mode observer
Trajectory tracking

ABSTRACT

This paper proposes a novel adaptive variable power sliding mode observer-based model predictive control (AVPSMO-MPC) method for the trajectory tracking of a Mecanum-wheeled mobile robot (MWMR) with external disturbances and model uncertainties. First, in the absence of disturbances and uncertainties, a model predictive controller that considers various physical constraints is designed based on the nominal dynamics model of the MWMR, which can transform the tracking problem into a constrained quadratic programming (QP) problem to solve the optimal control inputs online. Subsequently, to improve the anti-jamming ability of the MWMR, an AVPSMO is designed as a feedforward compensation controller to suppress the effects of external disturbances and model uncertainties during the actual motion of the MWMR, and the stability of the AVPSMO is proved via Lyapunov theory. The proposed AVPSMO-MPC method can achieve precise tracking control while ensuring that the constraints of MWMR are not violated in the presence of disturbances and uncertainties. Finally, comparative simulation cases are presented to demonstrate the effectiveness and robustness of the proposed method.

1. Introduction

The Mecanum-wheel mobile robot (MWMR) is a kind of omnidirectional mobile robot with four Mecanum wheels, which has excellent stability and mobility [1–3]. In recent years, the applications of MWMR in many fields have increased demand, such as industrial transportation, scientific research, home use and etc [4–6]. Trajectory tracking control is the key to enabling the system to autonomously achieve the desired state [7,8]. However, the MWMR is a nonlinear system with various constraints, making precise tracking control difficult to achieve [9].

To overcome these control difficulties, a variety of control algorithms have been developed for the trajectory tracking control of the MWMR, such as sliding mode control [10] and fuzzy control [11]. In [10], an adaptive integral terminal sliding mode control algorithm was proposed for trajectory tracking in the MWMR. To improve the movement accuracy and stability of the MWMR, a fuzzy adaptive proportion integration differentiation control method was presented and experimentally verified [11]. Although these studies performed well, they were not optimal control algorithms. Compared to non-optimal control approaches, model predictive control (MPC) is an optimal control approach, which can effectively deal with various system constraints. Note that it is necessary to consider physical constraints to achieve the desired control effect [12].

Owing to its ability to handle various complex constraints, MPC is widely used in robot control [13–15]. To simultaneously satisfy state and input constraints, a model-predictive fault-tolerant controller was designed for the tracking mission of the MWMR [16]. In [17], an algorithm that incorporates the learned barrier function into nonlinear MPC was proposed for multiple nonholonomic wheeled mobile robots to ensure the robots' safe navigation. A robust MPC method was developed to implement trajectory tracking control and simultaneously deal with various constraints of the MWMR [18]. In [19], a hierarchical MPC structure was presented, which simultaneously considers the non-minimal phase property of their newly designed wheeled bipedal robot, achieving precise pose tracking. In addition, a distributed MPC was designed to form multiple MWMRs with variable relative configurations [20]. Although MPC can effectively address

* Corresponding author at: School of Automation Science and Engineering, South China University of Technology, Guangzhou 510641, Guangdong, China.
E-mail addresses: dlwang@stu.edu.cn (D. Wang), andygao_scut@163.com (Y. Gao), weiwu@scut.edu.cn (W. Wei), yuqiuda@163.com (Q. Yu), weiyuhai888@126.com (Y. Wei), liwj@stu.edu.cn (W. Li), fanzhun@uestc.edu.cn (Z. Fan).

https://doi.org/10.1016/j.isatra.2024.05.050
Received 23 October 2022; Received in revised form 30 May 2024; Accepted 30 May 2024
Available online 1 June 2024

the constraint problem of mobile robots, it often relies on accurate model information [21]. When the robot model is not accurate, MPC may fail to achieve the desired control effect [22]. It is well known that the MWMR has a precise and complicated wheel-train structure; therefore, mechanical errors may lead to model uncertainties. Additionally, the control performance of most motion systems is affected by unknown disturbances that may exist in various real-world environments [23–25]. Most existing research on MWMR uses only the nominal model; however, the kinematics and dynamics of mobile robots can be perturbed by disturbances and uncertainties [26,27]. To achieve precise control, it is particularly important to consider the unknown disturbances and model uncertainties [28].

To solve these control problems, many scholars have conducted in-depth studies and proposed various solutions [29]. The sliding mode observer (SMO) is generally regarded as a powerful method. A control strategy based on SMO can effectively eliminate the influence of unknown disturbances and improve the control performance of the system [30]. In the study reported in [31], a novel control method based on a sliding mode disturbance observer was studied for the tracking problem of robot manipulators with model uncertainties and disturbances. Furthermore, a robust predictive controller based on a sliding mode disturbance observer was designed for permanent-magnet synchronous motor drive systems [32]. However, the discontinuous signum function introduced by the traditional SMO inevitably leads to high-frequency chattering of the system [33–35]. Due to their characteristics of reaching a stable state within a limited time and weaken the influence caused by chattering, high-order SMOs have attracted extensive attention from researchers [36]. In the study reported in [37], a closed-loop control strategy based on a fuzzy second-order SMO was adopted to realize the trajectory tracking control of a two-link robot. To suppress chattering, in [38], a super-twisting algorithm was introduced in the design of the SMO to approximate unknown disturbances, which improved the control effect of the system. It should be noted that high-order SMO greatly improves the control performance, but can weaken chattering only to a certain extent. Introducing a saturation function is an effective method for eliminating the effects of chattering [39]. In [40], a speed control strategy based on the SMO was investigated, in which the signum function was replaced with a sigmoid function based on a variable boundary layer. Moreover, an adaptive sliding mode control method was designed to realize the trajectory tracking control of differential-driving mobile robots with uncertain parameters by introducing a saturation function into the reaching law [41]. In [42], to improve the robustness of the system, a saturation function was introduced in the SMO design to eliminate the influence of chattering, and an adaptive sliding mode strategy was proposed to improve the tracking accuracy and response rate of the system. The above research results indicate that the SMO-based control algorithm can improve the anti-jamming capabilities and achieve a better control performance. However, to the best of our knowledge, although there have been a lot of research results, a trajectory tracking method that simultaneously considers the constraints and unknown disturbances of MWMR has not yet been fully studied. Inspired by the above research results, a model predictive control strategy based on a sliding mode observer (SMO-MPC) is beneficial for designing a tracking controller that considers these factors.

In this paper, an improved adaptive variable power SMO-based MPC algorithm is proposed to perform the desired trajectory tracking control for the MWMR with disturbances and uncertainties. By using the ability of the sliding mode observer based on adaptive variable power reaching law (AVPSMO) to estimate the lumped disturbances of the system, a feedforward compensation controller based on MPC is designed to suppress the effects of lumped disturbances. The proposed AVPSMO-MPC can improve tracking performance and robustness. The novelty of this study lies in the following aspects:

(1) The proposed method can deal with not only kinematic constraints but also dynamic constraints.

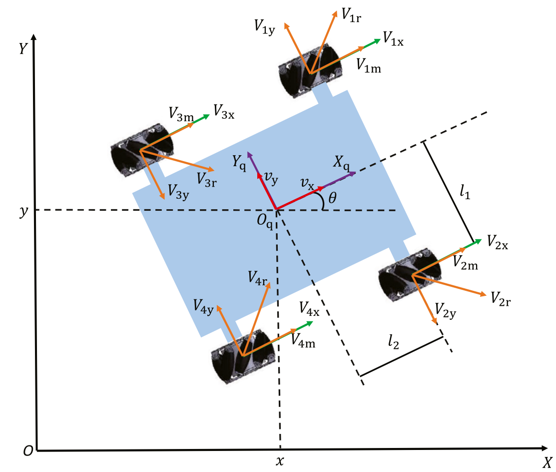

Fig. 1. The model of the Mecanum-wheeled mobile robot.

(2) Compared with traditional MPC, AVPSMO-MPC can not only deal with physical constraints effectively but also eliminate the effects of unknown disturbances and uncertainties.
(3) Compared with the traditional observer, the proposed AVPSMO can eliminate the influence of chattering and improve the convergence rate.

2. Problem formation

The MWMR is mainly composed of four Mecanum wheels which can be driven by independent motors. The Mecanum wheel has two degrees of freedom, namely the rotation around the axle and the translation in the direction orthogonal to the axis of the roller. By controlling the rotate velocity and steering of the four wheels, the robot can achieve omnidirectional movement.

2.1. Kinematics of MWMR

The motion schematic of the robot is shown in Fig. 1, where XOY and $X_qO_qY_q$ respectively represent the inertial coordinate system and robot coordinate system. We can express the resultant velocities of the wheels in the robot frame as:

$$\begin{aligned} V_{ix} &= V_{im} + V_{ir}\cos(\alpha_i), \\ V_{iy} &= V_{ir}\sin(\alpha_i), \end{aligned} \tag{1}$$

where $\alpha_1 = \alpha_4 = 45°$ and $\alpha_2 = \alpha_3 = -45°$ denote the offset angle of the rollers; V_{ix} and V_{iy} represent the resultant velocities of the wheels along the x-axis and y-axis respectively, while V_{im} and V_{ir} represent the tangential velocities of the free moving roller and the translational velocities of the wheels respectively, $i = 1, 2, 3, 4$. Define the distances between the wheels with the center of robot as L and l. Then, the correlation between the velocities of wheels and robot body can be established as:

$$\begin{bmatrix} V_{1x} \\ V_{2x} \\ V_{3x} \\ V_{4x} \end{bmatrix} = v_x + \omega \begin{bmatrix} -l \\ l \\ -l \\ l \end{bmatrix}, \begin{bmatrix} V_{1y} \\ V_{2y} \\ V_{3y} \\ V_{4y} \end{bmatrix} = v_y + \omega \begin{bmatrix} L \\ L \\ -L \\ -L \end{bmatrix}, \tag{2}$$

where the vector $[v_x, v_y, \omega]^T$ represent the velocities of the robot along x_q, y_q and the rotation velocity around the geometric center of the body.

By solving Eqs. (1) and (2), we can obtain the relation between the body velocities of the MWMR and the angular velocities of four wheels can be calculated as:

$$\begin{bmatrix} v_x \\ v_y \\ \omega \end{bmatrix} = \boldsymbol{J}_r \begin{bmatrix} w_1 \\ w_2 \\ w_3 \\ w_4 \end{bmatrix}, \tag{3}$$

where

$$\boldsymbol{J}_r = \frac{r}{4} \begin{bmatrix} 1 & 1 & 1 & 1 \\ -1 & 1 & 1 & -1 \\ \frac{-1}{l+L} & \frac{1}{l+L} & \frac{-1}{l+L} & \frac{1}{l+L} \end{bmatrix} \tag{4}$$

denotes the Jacobian matrix. The variable r is the radius of the Mecanum wheels, while $[w_1, w_2, w_3, w_4]^{\mathrm{T}}$ denote the velocities of four wheels.

Then, the nominal kinematics model of the robot can be written as:

$$\begin{bmatrix} \dot{x} \\ \dot{y} \\ \dot{\varphi} \end{bmatrix} = \begin{bmatrix} \cos(\varphi) & -\sin(\varphi) & 0 \\ \sin(\varphi) & \cos(\varphi) & 0 \\ 0 & 0 & 1 \end{bmatrix} \begin{bmatrix} v_x \\ v_y \\ \omega \end{bmatrix}, \tag{5}$$

where $[x, y, \varphi]^{\mathrm{T}}$ denotes the position and direction angle of robot in the inertial coordinate system.

2.2. Dynamics of MWMR

The nominal dynamics model of MWMR without considering friction can derived by using Lagrange equation. The kinetic energy equation of MWMR is given as follow [43]:

$$K = \frac{1}{2} m(v_x^2 + v_y^2) + \frac{1}{2} J_z \omega^2 + \frac{1}{2} J_\omega(\dot{\theta}_1^2 + \dot{\theta}_2^2 + \dot{\theta}_3^2 + \dot{\theta}_4^2), \tag{6}$$

where $\dot{\theta}_i = \omega_i$, $i = 1, 2, 3, 4$; m denotes the total mass of the MWMR; J_z and J_ω denote the MWMR moment and the wheels moment of inertia around their center of revolution. Noted that viscous friction can cause certain energy loss:

$$D = \frac{1}{2} D_\theta(\dot{\theta}_1^2 + \dot{\theta}_2^2 + \dot{\theta}_3^2 + \dot{\theta}_4^2), \tag{7}$$

where D_θ represents the viscous friction coefficient between the wheels and the road surface during robot movement. The Lagrangian function is expressed as:

$$L = K - V, \tag{8}$$

where $V = 0$ represents the potential energy of the robot in the plane of motion. Then, the use of the Lagrangian function yields [9]:

$$\begin{aligned} 2(\boldsymbol{\tau} - \boldsymbol{f}) - \frac{\partial D_\theta \sum_{i=1}^4 \dot{\theta}_i^2}{\partial \dot{\boldsymbol{\theta}}} &= \frac{\partial}{\partial t} \frac{\partial(m(v_x^2 + v_y^2) + J_z\omega^2 + J_\omega \sum_{i=1}^4 \dot{\theta}_i^2)}{\partial \dot{\boldsymbol{\theta}}} \\ &\quad - \frac{\partial(m(v_x^2 + v_y^2) + J_z\omega^2 + J_\omega \sum_{i=1}^4 \dot{\theta}_i^2)}{\partial \boldsymbol{\theta}} \end{aligned} \tag{9}$$

where $\boldsymbol{\theta} = [\theta_1, \theta_2, \theta_3, \theta_4]^{\mathrm{T}}$; $\boldsymbol{f}$ represents the static friction; The vector $\boldsymbol{\tau} = [\tau_1, \tau_2, \tau_3, \tau_4]^{\mathrm{T}}$ denotes the external generalized force generated by the DC motor corresponding to the four wheels.

Substituting (3), (5) into (9), one obtains:

$$\boldsymbol{\tau} = \boldsymbol{M}\ddot{\boldsymbol{\theta}} + D_\theta \dot{\boldsymbol{\theta}} + \boldsymbol{f}, \tag{10}$$

where

$$\begin{aligned} \boldsymbol{M} &= \begin{bmatrix} \boldsymbol{A}_j + \boldsymbol{B}_j + \boldsymbol{J}_\omega & -\boldsymbol{B}_j & \boldsymbol{B}_j & \boldsymbol{A}_j - \boldsymbol{B}_j \\ -\boldsymbol{B}_j & \boldsymbol{A}_j + \boldsymbol{B}_j + \boldsymbol{J}_\omega & \boldsymbol{A}_j - \boldsymbol{B}_j & \boldsymbol{B}_j \\ \boldsymbol{B}_j & \boldsymbol{A}_j - \boldsymbol{B}_j & \boldsymbol{A}_j + \boldsymbol{B}_j + \boldsymbol{J}_\omega & -\boldsymbol{B}_j \\ \boldsymbol{A}_j - \boldsymbol{B}_j & -\boldsymbol{B}_j & -\boldsymbol{B}_j & \boldsymbol{A}_j + \boldsymbol{B}_j + \boldsymbol{J}_\omega \end{bmatrix}, \\ \boldsymbol{A}_j &= \frac{mr^2}{8}, \quad \boldsymbol{B}_j = \frac{J_z r^2}{16(L+l)}. \end{aligned} \tag{11}$$

Differentiating (2) and substituting (1), (10), the nominal dynamics model of the robot can be written as:

$$\begin{aligned} \begin{bmatrix} \ddot{x} \\ \ddot{y} \\ \ddot{\varphi} \end{bmatrix} &= -(\boldsymbol{J}^+(\varphi)\dot{\boldsymbol{J}}(\varphi) + D_\theta \boldsymbol{J}^+(\varphi)\boldsymbol{M}^{-1}\boldsymbol{J}(\varphi)) \begin{bmatrix} \dot{x} \\ \dot{y} \\ \dot{\varphi} \end{bmatrix} \\ &\quad + r\boldsymbol{J}^+(\varphi)\boldsymbol{M}^{-1}(\boldsymbol{\tau} - \boldsymbol{f}) \end{aligned} \tag{12}$$

where $\boldsymbol{J}^+(\varphi)$ and $\dot{\boldsymbol{J}}(\varphi)$ respectively represent the generalized inverse and the derivative matrix of $\boldsymbol{J}(\varphi)$, and

$$\begin{aligned} \boldsymbol{J}(\varphi) &= \begin{bmatrix} \sqrt{2}\sin(\varphi_a) & -\sqrt{2}\cos(\varphi_a) & -(l+L) \\ \sqrt{2}\cos(\varphi_a) & \sqrt{2}\sin(\varphi_a) & (l+L) \\ \sqrt{2}\cos(\varphi_a) & \sqrt{2}\sin(\varphi_a) & -(l+L) \\ \sqrt{2}\sin(\varphi_a) & -\sqrt{2}\cos(\varphi_a) & (l+L) \end{bmatrix}, \\ \varphi_a &= \varphi + \frac{\pi}{4}. \end{aligned} \tag{13}$$

Defining a state variable $\boldsymbol{x} = [x, y, \varphi, \dot{x}, \dot{y}, \dot{\varphi}]^{\mathrm{T}}$ and system control input u, the system state equation of MWMR can be obtained as follow:

$$\dot{\boldsymbol{x}} = \boldsymbol{A}\boldsymbol{x} + \boldsymbol{B}\boldsymbol{u}, \tag{14}$$

where

$$\begin{aligned} \boldsymbol{A} &= \begin{bmatrix} \boldsymbol{0} & \boldsymbol{E} \\ \boldsymbol{0} & -(\boldsymbol{J}^+(\varphi)\dot{\boldsymbol{J}}(\varphi) + D_\theta \boldsymbol{J}^+(\varphi)\boldsymbol{M}^{-1}\boldsymbol{J}(\varphi)) \end{bmatrix} \in \mathbb{R}^{6\times6}, \\ \boldsymbol{B} &= \begin{bmatrix} \boldsymbol{0} \\ r\boldsymbol{J}^+(\varphi)\boldsymbol{M}^{-1} \end{bmatrix} \in \mathbb{R}^{6\times4}, \end{aligned} \tag{15}$$

and $\boldsymbol{E}$ represents the identity matrix of the corresponding dimension.

Moreover, it is well known that to realize desired control effect, unknown disturbances and model uncertainties need to be considered. In order to derive the kinematic model of MWMR in the presence of external disturbances and model uncertainties, the following assumption need to be made:

Assumption 1. The unknown disturbances and model uncertainties in the system are all bounded.

Then, the relationship between body velocities and the velocities of wheels considering the unknown disturbances and model uncertainties can be written as follows:

$$\begin{bmatrix} v_x \\ v_y \\ \omega \end{bmatrix} = \boldsymbol{J}_r \begin{bmatrix} w_1 \\ w_2 \\ w_3 \\ w_4 \end{bmatrix} + \begin{bmatrix} f_x \\ f_y \\ f_\omega \end{bmatrix}, \tag{16}$$

where $[f_x, f_y, f_\omega]^{\mathrm{T}}$ denotes the lumped disturbances including unknown disturbances and model uncertainties in different velocity directions of the robot centroid. Then, the kinematic model can be written as:

$$\begin{bmatrix} \dot{x} \\ \dot{y} \\ \dot{\varphi} \end{bmatrix} = \begin{bmatrix} \cos(\varphi) & -\sin(\varphi) & 0 \\ \sin(\varphi) & \cos(\varphi) & 0 \\ 0 & 0 & 1 \end{bmatrix} \left(\boldsymbol{J}_r \begin{bmatrix} w_1 \\ w_2 \\ w_3 \\ w_4 \end{bmatrix} + \begin{bmatrix} f_x \\ f_y \\ f_\omega \end{bmatrix} \right). \tag{17}$$

Remark 1. Most control algorithms for MWMR can use the nominal kinematics model (5) to achieve ideal trajectory tracking control; however, the effects of lumped disturbances cannot be ignored in practical implementations. The main purpose of this paper is to design a composite controller consisting of a nominal MPC and feedforward AVPSMO, to eliminate the influence of lumped disturbances and ensure that the system constraints are not destroyed. The nominal MPC uses the nominal dynamics model (14) to obtain an ideal tracking trajectory without considering the disturbances and uncertainties. The AVPSMO is designed to approximate unknown terms, to realize disturbance compensation and eliminate the influence of lumped disturbances.

3. Model predictive control

The essence of MPC is a rolling optimization algorithm. At each sampling instant, the MPC needs to solve the optimization problem online iteratively to obtain the control sequence. In this section, the nominal dynamics model (12) of the robot is used to design the model predictive controller. The discrete expression of system (14) is as follows:

$$\boldsymbol{x}_{k+1} = \boldsymbol{G}_k \boldsymbol{x}_k + \boldsymbol{H}_k \boldsymbol{u}_k, \tag{18}$$

where

$$\boldsymbol{G}_k = (\boldsymbol{E} + T\boldsymbol{A}),\ \ \boldsymbol{H}_k = T\boldsymbol{B}. \tag{19}$$

The notation T is the sampling time. Define N_{p} and N_{c} as the prediction horizon and control horizon of the system, respectively. Then, the following cost function can be formulated:

$$J = \sum_{j=1}^{N_{\mathrm{p}}} \| \boldsymbol{x}_{k+j|k} - \boldsymbol{r}_{k+j|k} \|_{\boldsymbol{Q}}^2 + \sum_{j=0}^{N_{\mathrm{c}}-1} \| \Delta \boldsymbol{u}_{k+j|k} \|_{\boldsymbol{P}}^2 \tag{20}$$

where $\boldsymbol{Q}$ and $\boldsymbol{P}$ denote positive definite matrix of corresponding dimension. The notation $\boldsymbol{x}_{k+j|k}$ and $\boldsymbol{r}_{k+j|k}$ denote the predicted state and the set desired value at instant $k+j$ respectively. The input increment vector $\Delta \boldsymbol{u}_{k+j|k} = \boldsymbol{u}_{k+j|k} - \boldsymbol{u}_{k+j-1|k}$, where $\boldsymbol{u}_{k+j|k}$ is the control input vector at time instant $k+j$.

Then, define the following prediction sequence:

$$\begin{aligned}
&\bar{\boldsymbol{x}}_k \triangleq [\boldsymbol{x}_{k+1|k}^{\mathrm{T}}, \boldsymbol{x}_{k+2|k}^{\mathrm{T}}, \ldots, \boldsymbol{x}_{k+N_{\mathrm{p}}|k}^{\mathrm{T}}]^{\mathrm{T}} \in \mathbb{R}^{6N_{\mathrm{p}}} \\
&\bar{\boldsymbol{r}}_k \triangleq [\boldsymbol{r}_{k+1|k}^{\mathrm{T}}, \boldsymbol{r}_{k+2|k}^{\mathrm{T}}, \ldots, \boldsymbol{r}_{k+N_{\mathrm{p}}|k}^{\mathrm{T}}]^{\mathrm{T}} \in \mathbb{R}^{6N_{\mathrm{p}}} \\
&\bar{\boldsymbol{u}}_k \triangleq [\boldsymbol{u}_{k|k}^{\mathrm{T}}, \boldsymbol{u}_{k+1|k}^{\mathrm{T}}, \ldots, \boldsymbol{u}_{k+N_{\mathrm{c}}-1|k}^{\mathrm{T}}]^{\mathrm{T}} \in \mathbb{R}^{4N_{\mathrm{c}}} \\
&\triangle \bar{\boldsymbol{u}}_k \triangleq [\triangle \boldsymbol{u}_{k|k}^{\mathrm{T}}, \triangle \boldsymbol{u}_{k+1|k}^{\mathrm{T}}, \ldots, \triangle \boldsymbol{u}_{k+N_{\mathrm{c}}-1|k}^{\mathrm{T}}]^{\mathrm{T}} \in \mathbb{R}^{4N_{\mathrm{c}}}
\end{aligned} \tag{21}$$

subject to

$$\begin{aligned}
&\bar{\boldsymbol{x}}_{\min} \le \bar{\boldsymbol{x}}_k \le \bar{\boldsymbol{x}}_{\max}, \\
&\bar{\boldsymbol{u}}_{\min} \le \bar{\boldsymbol{u}}_k \le \bar{\boldsymbol{u}}_{\max}, \\
&\triangle \bar{\boldsymbol{u}}_{\min} \le \triangle \bar{\boldsymbol{u}}_k \le \triangle \bar{\boldsymbol{u}}_{\max},
\end{aligned} \tag{22}$$

where $\bar{\boldsymbol{x}}_{\min}$, $\bar{\boldsymbol{x}}_{\max}$, $\bar{\boldsymbol{u}}_{\min}$, $\bar{\boldsymbol{u}}_{\max}$, $\triangle \bar{\boldsymbol{u}}_{\min}$ and $\triangle \bar{\boldsymbol{u}}_{\max}$ are the corresponding lower and upper bounds of variables. Then, the prediction of states at the future moment can be calculated as:

$$\begin{aligned}
&\boldsymbol{x}_{k+1|k} = \boldsymbol{G}_k \boldsymbol{x}_{k|k} + \boldsymbol{H}_k \boldsymbol{u}_{k|k} \\
&\boldsymbol{x}_{k+2|k} = \boldsymbol{G}_{k+1} \boldsymbol{x}_{k+1|k} + \boldsymbol{H}_{k+1} \boldsymbol{u}_{k+1|k} \\
&\qquad\vdots \\
&\boldsymbol{x}_{k+N_{\mathrm{p}}|k} = \boldsymbol{G}_{k+N_{\mathrm{p}}-1} \boldsymbol{x}_{k+N_{\mathrm{p}}-1|k} + \boldsymbol{H}_{k+N_{\mathrm{p}}-1} \boldsymbol{u}_{k+N_{\mathrm{p}}-1|k}
\end{aligned} \tag{23}$$

Then, Eq. (23) can be rewritten as the follow compact form:

$$\bar{\boldsymbol{x}}_k = \boldsymbol{M}_k \boldsymbol{x}_k + \boldsymbol{N}_k \boldsymbol{u}_{k-1} + \boldsymbol{Z}_k \triangle \bar{\boldsymbol{u}}_k, \tag{24}$$

where

$$\boldsymbol{M}_k = \begin{bmatrix} \boldsymbol{G}_k \\ \boldsymbol{G}_{k+1}\boldsymbol{G}_k \\ \vdots \\ \overleftarrow{\prod}_{i=k}^{i=k+N_{\mathrm{p}}-1} \boldsymbol{G}_i \end{bmatrix} \in \mathbb{R}^{6N_{\mathrm{p}} \times 6},$$

$$\boldsymbol{N}_k = \begin{bmatrix} \boldsymbol{H}_k \\ \boldsymbol{H}_{k+1} + \boldsymbol{G}_{k+1}\boldsymbol{H}_k \\ \vdots \\ \boldsymbol{H}_{k+N_{\mathrm{p}}-1} + \overleftarrow{\prod}_{i=k+1}^{i=k+N_{\mathrm{p}}-1} \boldsymbol{G}_i \boldsymbol{H}_k + \cdots + \overleftarrow{\prod}_{i=k+N_{\mathrm{p}}-1}^{i=k+N_{\mathrm{p}}-1} \boldsymbol{G}_i \boldsymbol{H}_{k+N_{\mathrm{p}}-2} \end{bmatrix} \in \mathbb{R}^{6N_{\mathrm{p}} \times 4},$$

$$\boldsymbol{Z}_k = \begin{bmatrix} \boldsymbol{H}_k & \cdots & \boldsymbol{0} \\ \boldsymbol{H}_{k+1} + \boldsymbol{G}_{k+1}\boldsymbol{H}_k & \cdots & \boldsymbol{0} \\ \vdots & \ddots & \vdots \\ \boldsymbol{H}_{k+N_{\mathrm{p}}-1} + \overleftarrow{\prod}_{i=k+1}^{i=k+N_{\mathrm{p}}-1} \boldsymbol{G}_i \boldsymbol{H}_k + \cdots + \overleftarrow{\prod}_{i=k+N_{\mathrm{p}}-1}^{i=k+N_{\mathrm{p}}-1} \boldsymbol{G}_i \boldsymbol{H}_{k+N_{\mathrm{p}}-2} & \cdots & \boldsymbol{H}_{k+N_{\mathrm{p}}-1} + \overleftarrow{\prod}_{i=k+N_{\mathrm{c}}+1}^{i=k+N_{\mathrm{p}}-1} \boldsymbol{G}_i \boldsymbol{H}_{k+N_{\mathrm{c}}-1} + \cdots + \overleftarrow{\prod}_{i=k+N_{\mathrm{p}}-1}^{i=k+N_{\mathrm{p}}-1} \boldsymbol{G}_i \boldsymbol{H}_{k+N_{\mathrm{p}}-2} \end{bmatrix} \in \mathbb{R}^{6N_{\mathrm{p}} \times 4N_{\mathrm{c}}}. \tag{25}$$

The notation $\overleftarrow{\prod}$ means multiplying to the left. Then, the cost function (20) can be transformed into the following optimization problem:

$$\min J(k) = \| \boldsymbol{M}_k \boldsymbol{x}_k + \boldsymbol{N}_k \boldsymbol{u}_{k-1} + \boldsymbol{Z}_k \triangle \bar{\boldsymbol{u}}_k - \bar{\boldsymbol{r}}_k \|_{\boldsymbol{Q}}^2 + \| \triangle \bar{\boldsymbol{u}}_k \|_{\boldsymbol{P}}^2, \tag{26}$$

subjected to

$$\begin{aligned}
&\bar{\boldsymbol{x}}_{\min} \le \boldsymbol{M}_k \boldsymbol{x}_k + \boldsymbol{N}_k \boldsymbol{u}_{k-1} + \boldsymbol{Z}_k \triangle \tilde{\boldsymbol{u}}_k \le \bar{\boldsymbol{x}}_{\max}, \\
&\bar{\boldsymbol{u}}_{\min} \le \boldsymbol{U}_{k-1} + \bar{\boldsymbol{E}} \triangle \bar{\boldsymbol{u}}_k \le \bar{\boldsymbol{u}}_{\max}, \\
&\triangle \bar{\boldsymbol{u}}_{\min} \le \triangle \bar{\boldsymbol{u}}_k \le \triangle \bar{\boldsymbol{u}}_{\max},
\end{aligned} \tag{27}$$

where

$$\boldsymbol{U}_{k-1} = 1_{N_{\mathrm{c}}} \bigotimes \boldsymbol{u}_{k-1} \in \mathbb{R}^{4N_{\mathrm{c}}}, \quad \bar{\boldsymbol{E}} = \begin{bmatrix} \boldsymbol{E} & 0 & \cdots & 0 \\ \boldsymbol{E} & \boldsymbol{E} & \cdots & 0 \\ \vdots & \vdots & \ddots & \vdots \\ \boldsymbol{E} & \boldsymbol{E} & \boldsymbol{E} & \boldsymbol{E} \end{bmatrix} \in \mathbb{R}^{4N_{\mathrm{c}} \times 4N_{\mathrm{c}}}, \tag{28}$$

The problem (26) can be transformed into a constrained QP problem as follows:

$$\min \frac{1}{2} \triangle \bar{\boldsymbol{u}}_k^{\mathrm{T}} \boldsymbol{\gamma} \triangle \bar{\boldsymbol{u}}_k + \boldsymbol{\kappa}^{\mathrm{T}} \triangle \bar{\boldsymbol{u}}_k, \tag{29}$$

subject to

$$\boldsymbol{W} \triangle \bar{\boldsymbol{u}}_k \leqslant \boldsymbol{h}, \tag{30}$$

where

$$\begin{aligned}
&\boldsymbol{\gamma} = 2(\boldsymbol{Z}_k^{\mathrm{T}} \boldsymbol{Q} \boldsymbol{Z}_k + \boldsymbol{P}) \in \mathbb{R}^{4N_{\mathrm{c}} \times 4N_{\mathrm{c}}}, \\
&\boldsymbol{\kappa} = 2\boldsymbol{Z}_k^{\mathrm{T}} \boldsymbol{Q} (\boldsymbol{M}_k \boldsymbol{x}_k + \boldsymbol{N}_k \boldsymbol{u}_{k-1} - \bar{\boldsymbol{r}}_k) \in \mathbb{R}^{4N_{\mathrm{c}}}, \\
&\boldsymbol{W} = \begin{bmatrix} \boldsymbol{Z}_k \\ -\boldsymbol{Z}_k \\ \bar{\boldsymbol{E}} \\ -\bar{\boldsymbol{E}} \\ \tilde{\boldsymbol{E}} \\ -\tilde{\boldsymbol{E}} \end{bmatrix} \in \mathbb{R}^{(12N_{\mathrm{p}} + 16N_{\mathrm{c}}) \times 4N_{\mathrm{c}}}, \\
&\tilde{\boldsymbol{E}} = \begin{bmatrix} 1 & 0 & 0 & 0 \cdots & 0 \\ 0 & 1 & 0 & 0 \cdots & 0 \\ 0 & 0 & 1 & 0 \cdots & 0 \\ \vdots & \vdots & \ddots & \vdots & \vdots \\ 0 & 0 & 0 & \cdots & 1 \end{bmatrix} \in \mathbb{R}^{4N_{\mathrm{c}} \times 4N_{\mathrm{c}}}, \\
&\boldsymbol{h} = \begin{bmatrix} \bar{\boldsymbol{x}}_{\max} - \boldsymbol{M}_k \boldsymbol{x}_k - \boldsymbol{N}_k \boldsymbol{u}_{k-1} \\ -\bar{\boldsymbol{x}}_{\min} + \boldsymbol{M}_k \boldsymbol{x}_k + \boldsymbol{N}_k \boldsymbol{u}_{k-1} \\ \bar{\boldsymbol{u}}_{\max} - \boldsymbol{U}_{k-1} \\ -\bar{\boldsymbol{u}}_{\min} + \boldsymbol{U}_{k-1} \\ \triangle \bar{\boldsymbol{u}}_{\max} \\ -\triangle \bar{\boldsymbol{u}}_{\min} \end{bmatrix} \in \mathbb{R}^{12N_{\mathrm{p}} + 16N_{\mathrm{c}}}.
\end{aligned} \tag{31}$$

4. Sliding mode observer

In this section, an improved AVPSMO is designed to approximate the lumped disturbances in the kinematics model of robot. And use the disturbance estimations to eliminate the influence of disturbances on the system to improve the robustness of the system. The kinematics model (17) can be rearranged as:

$$\dot{\boldsymbol{z}} = \bar{\boldsymbol{B}}\boldsymbol{v} + \boldsymbol{D}\boldsymbol{f}, \tag{32}$$

where

$$\begin{aligned}\bar{\boldsymbol{B}} &= \frac{r}{4}\begin{bmatrix}\cos(\varphi) & -\sin(\varphi) & 0\\ \sin(\varphi) & \cos(\varphi) & 0\\ 0 & 0 & 1\end{bmatrix}\begin{bmatrix}1 & 1 & 1 & 1\\ -1 & 1 & 1 & -1\\ \frac{-1}{l+L} & \frac{1}{l+L} & \frac{-1}{l+L} & \frac{1}{l+L}\end{bmatrix},\\ \boldsymbol{D} &= \begin{bmatrix}\cos(\varphi) & -\sin(\varphi) & 0\\ \sin(\varphi) & \cos(\varphi) & 0\\ 0 & 0 & 1\end{bmatrix},\end{aligned} \tag{33}$$

$\boldsymbol{v} = [w_1\ w_2\ w_3\ w_4]^{\mathrm{T}}$ and $\boldsymbol{z} = [x\ y\ \varphi]^{\mathrm{T}}$. Then, the sliding surface can be designed as:

$$\boldsymbol{s} = \boldsymbol{z} - \hat{\boldsymbol{z}}, \tag{34}$$

where $\boldsymbol{s} = [s_1, s_2, s_3]^{\mathrm{T}}$, and $\hat{\boldsymbol{z}} = [\hat{x}, \hat{y}, \hat{\varphi}]^{\mathrm{T}}$ denote the estimate value of the position and direction angle. Then, the adaptive variable power reaching law can be designed as:

$$\dot{\boldsymbol{s}} = -\boldsymbol{K}_1\boldsymbol{s} - (\boldsymbol{K}_2 + \boldsymbol{K}_3|\boldsymbol{s}|^{\lambda_1} + \boldsymbol{K}_4|\boldsymbol{s}|^{\lambda_2})\mathbf{sat}(\boldsymbol{s}), \tag{35}$$

where $\mathbf{sat}(\boldsymbol{s}) \triangleq [\mathrm{sat}(s_1), \mathrm{sat}(s_2), \mathrm{sat}(s_3)]^{\mathrm{T}}$, in which the saturation function $\mathrm{sat}(s_i), i = 1, 2, 3$ can be designed as: $\mathrm{sat}(s_i) = \begin{cases}1, & s_i/\chi > 1\\ s_i/\chi, & -1 \le s_i/\chi \le 1\\ -1, & s_i/\chi < -1\end{cases}$, $\chi > 0$ is the thickness of the boundary layer. Moreover, $\boldsymbol{\lambda}_1 = \mathrm{diag}(\lambda_{11}, \lambda_{12}, \lambda_{13})$ and $\boldsymbol{\lambda}_2 = \mathrm{diag}(\lambda_{21}, \lambda_{22}, \lambda_{23})$ are the corresponding variable exponential power matrices, and

$$\begin{aligned}&\boldsymbol{\lambda}_1 \triangleq \eta_1 \cdot \boldsymbol{E} \cdot \mathbf{tanh}(|\boldsymbol{s}|^{\delta})|\boldsymbol{s}| + \eta_2\boldsymbol{E},\\ &\boldsymbol{\lambda}_2 \triangleq 0.5(\eta_3\boldsymbol{E} + \boldsymbol{E}) + 0.5(\eta_3\boldsymbol{E} - \boldsymbol{E})\mathbf{sgn}(|\boldsymbol{s}| - \boldsymbol{E}),\\ &|\boldsymbol{s}| \triangleq \begin{bmatrix}|s_1| & 0 & 0\\ 0 & |s_2| & 0\\ 0 & 0 & |s_3|\end{bmatrix},\\ &|\boldsymbol{s}|^{\lambda_i} \triangleq \begin{bmatrix}|s_1|^{\lambda_{i1}} & 0 & 0\\ 0 & |s_2|^{\lambda_{i2}} & 0\\ 0 & 0 & |s_3|^{\lambda_{i3}}\end{bmatrix},\\ &\mathbf{tanh}(|\boldsymbol{s}|^{\delta}) \triangleq \begin{bmatrix}tanh(|s_1|^{\delta}) & 0 & 0\\ 0 & \tanh(|s_2|^{\delta}) & 0\\ 0 & 0 & \tanh(|s_3|^{\delta})\end{bmatrix},\\ &\mathbf{sgn}(|\boldsymbol{s}| - \boldsymbol{E}) \triangleq \begin{bmatrix}\mathrm{sgn}(|s_1| - 1) & 0 & 0\\ 0 & \mathrm{sgn}(|s_2| - 1) & 0\\ 0 & 0 & \mathrm{sgn}(|s_3| - 1)\end{bmatrix},\end{aligned} \tag{36}$$

in which $\eta_1 > 1, 0 < \eta_2 < 1, \eta_3 > 1$, σ is a constant going to infinity and $\boldsymbol{K}_\iota = \mathrm{diag}(k_{\iota 1}, k_{\iota 2}, k_{\iota 3}), \iota = 1, 2, 3, 4$ is appropriate positive definite matrix. The adaptive laws of $\boldsymbol{K}_\iota$ can be designed as:

$$\begin{cases}\dot{k}_{11} = \xi_1 s_1^2,\\ \dot{k}_{12} = \xi_2 s_2^2,\\ \dot{k}_{13} = \xi_3 s_3^2,\end{cases} \begin{cases}\dot{k}_{21} = \varsigma_1 s_1 sat(s_1),\\ \dot{k}_{22} = \varsigma_2 s_2 sat(s_2),\\ \dot{k}_{23} = \varsigma_3 s_3 sat(s_3),\end{cases} \begin{cases}\dot{k}_{31} = \kappa_1|s_1|^{\lambda_{11}+1},\\ \dot{k}_{32} = \kappa_2|s_2|^{\lambda_{12}+1},\\ \dot{k}_{33} = \kappa_3|s_3|^{\lambda_{13}+1},\end{cases} \begin{cases}\dot{k}_{41} = \sigma_1|s_1|^{\lambda_{21}+1},\\ \dot{k}_{42} = \sigma_2|s_2|^{\lambda_{22}+1},\\ \dot{k}_{43} = \sigma_3|s_3|^{\lambda_{23}+1},\end{cases} \tag{37}$$

where $\xi_i, \varsigma_i, \kappa_i$ and σ_i are all positive constants.

Remark 2. The novel reaching law (35) can significantly improve the convergence rate whether the sliding surface $\boldsymbol{s}$ is close to or far from zero. When $|s_i| \ge 1, \lambda_{1i} = \eta_1|s_i| + \eta_2, \lambda_{2i} = \eta_3$, all terms play an important role in accelerating convergence. When $|s_i| < 1, \lambda_{1i} = \eta_2, \lambda_{2i} = 1$, the reaching rate is equal to a quick power reaching rate.

Then, the AVPSMO can be designed as:

$$\dot{\hat{\boldsymbol{z}}} = \bar{\boldsymbol{B}}\boldsymbol{v} + \boldsymbol{K}_1\boldsymbol{s} + (\boldsymbol{K}_2 + \boldsymbol{K}_3|\boldsymbol{s}|^{\lambda_1} + \boldsymbol{K}_4|\boldsymbol{s}|^{\lambda_2})\mathbf{sat}(\boldsymbol{s}) \tag{38}$$

By subtracting (38) from (32), the observation error can be obtained as:

$$\dot{\boldsymbol{s}} = \boldsymbol{D}\boldsymbol{f} - \boldsymbol{K}_1\boldsymbol{s} - (\boldsymbol{K}_2 + \boldsymbol{K}_3|\boldsymbol{s}|^{\lambda_1} + \boldsymbol{K}_4|\boldsymbol{s}|^{\lambda_2})\mathbf{sat}(\boldsymbol{s}) \tag{39}$$

Once the system reaches the sliding surface, then

$$\boldsymbol{s} = \dot{\boldsymbol{s}} = 0 \tag{40}$$

Combining (39) and (40), yields

$$\hat{\boldsymbol{f}} = \boldsymbol{D}^{-1}[\boldsymbol{K}_1\boldsymbol{s} + (\boldsymbol{K}_2 + \boldsymbol{K}_3|\boldsymbol{s}|^{\lambda_1} + \boldsymbol{K}_4|\boldsymbol{s}|^{\lambda_2})\mathbf{sat}(\boldsymbol{s})] \tag{41}$$

Theorem 1. *For the robot system (32), the unknown disturbances and uncertainties of the robot can be accurately estimated by the AVPSMO (38).*

Proof. Define $\bar{k}_{\iota 1}, \bar{k}_{\iota 2}, \bar{k}_{\iota 3}$ are the corresponding nominal values of $k_{\iota 1}, k_{\iota 2}, k_{\iota 3}$. Then, choose the following Lyapunov function:

$$V_i = \frac{1}{2}s_i^2 + \frac{1}{2\xi_i}\tilde{k}_{1i}^2 + \frac{1}{2\varsigma_i}\tilde{k}_{2i}^2 + \frac{1}{2\kappa_i}\tilde{k}_{3i}^2 + \frac{1}{2\sigma_i}\tilde{k}_{4i}^2 \tag{42}$$

where $\tilde{k}_{\iota i} = k_{\iota i} - \bar{k}_{\iota i}, \iota = 1, 2, 3, 4$, and $i = 1, 2, 3$. Obviously, the function V_i is positive definite. Define $\boldsymbol{d}_{\mathrm{dis}} = \boldsymbol{D}\boldsymbol{f} = [d_{1\mathrm{dis}}, d_{2\mathrm{dis}}, d_{3\mathrm{dis}}]^{\mathrm{T}}$. Then, differentiating Eq. (42) with respect to time yields

$$\begin{aligned}\dot{V}_i &= s_i\dot{s}_i + s_i^2\tilde{k}_{1i} + s_i\mathrm{sat}(s_i)\tilde{k}_{2i} + |s_i|^{\lambda_{1i}+1}\tilde{k}_{3i} + |s_i|^{\lambda_{2i}+1}\tilde{k}_{4i}\\ &= s_i[d_{i\mathrm{dis}} - k_{1i}s_i - k_{2i}\mathrm{sat}(s_i) - k_{3i}|s_i|^{\lambda_{1i}}\mathrm{sat}(s_i)\\ &\quad - k_{4i}|s_i|^{\lambda_{2i}}\mathrm{sat}(s_i)] + s_i^2\tilde{k}_{1i} + s_i\mathrm{sat}(s_i)\tilde{k}_{2i}\\ &\quad + |s_i|^{\lambda_{1i}+1}\tilde{k}_{3i} + |s_i|^{\lambda_{2i}+1}\tilde{k}_{4i}\\ &= s_i[d_{i\mathrm{dis}} - k_{3i}|s_i|^{\lambda_{1i}}\mathrm{sat}(s_i) - k_{4i}|s_i|^{\lambda_{2i}}\mathrm{sat}(s_i)]\\ &\quad - s_i^2\bar{k}_{1i} - s_i\mathrm{sat}(s_i)\bar{k}_{2i} + |s_i|^{\lambda_{1i}+1}\tilde{k}_{3i}\\ &\quad + |s_i|^{\lambda_{2i}+1}\tilde{k}_{4i}\\ &\le s_i[d_{i\mathrm{dis}} - k_{3i}|s_i|^{\lambda_{1i}}\mathrm{sat}(s_i) - k_{4i}|s_i|^{\lambda_{2i}}\mathrm{sat}(s_i)]\\ &\quad - s_i\mathrm{sat}(s_i)\bar{k}_{2i} + |s_i|^{\lambda_{1i}+1}\tilde{k}_{3i} + |s_i|^{\lambda_{2i}+1}\tilde{k}_{4i}\\ &\le |s_i d_{i\mathrm{dis}}| - k_{3i}|s_i|^{\lambda_{1i}+1}|\mathrm{sat}(s_i)| - k_{4i}|s_i|^{\lambda_{2i}+1}|\mathrm{sat}(s_i)|\\ &\quad - s_i\mathrm{sat}(s_i)\bar{k}_{2i} + |s_i|^{\lambda_{1i}+1}\tilde{k}_{3i} + |s_i|^{\lambda_{2i}+1}\tilde{k}_{4i}\end{aligned} \tag{43}$$

Note that when $|s_i| \ge \chi, i = 1, 2, 3$, yields

$$\begin{aligned}\dot{V}_i &\le |s_i||d_{i\mathrm{dis}}| - k_{3i}|s_i|^{\lambda_{1i}+1}|\mathrm{sat}(s_i)| - k_{4i}|s_i|^{\lambda_{2i}+1}|\mathrm{sat}(s_i)|\\ &\quad - s_i\mathrm{sat}(s_i)\bar{k}_{2i} + |s_i|^{\lambda_{1i}+1}k_{3i} + |s_i|^{\lambda_{2i}+1}k_{4i}\\ &= |s_i||d_{i\mathrm{dis}}| - s_i\mathrm{sat}(s_i)\bar{k}_{2i}\\ &= |s_i||d_{i\mathrm{dis}}| - |s_i|\bar{k}_{2i}\end{aligned} \tag{44}$$

According to *Assumption* 1, it can be deduced that $\boldsymbol{d}_{\mathrm{dis}}$ is bounded, so the nominal values of definite matrix $\boldsymbol{K}_2$ can be designed to make $|d_{i\mathrm{dis}}| < \bar{k}_{2i}, i = 1, 2, 3$. In this case, it is easy to prove $\dot{V}_i < 0$, indicating that all sliding mode variables $s_i, i = 1, 2, 3$ can converge to the inside of boundary layer. When the thickness of boundary layer goes to zero, the sliding mode variable s_i converge to zero. Therefore, the system is stable.

This ends the proof. □

Remark 3. To improve the performance of the observer, this paper has made the following improvements to the AVPSMO: (*i*) The variable power reaching law that combines the advantages of the double power reaching law and the exponential reaching law is introduced. (*ii*) In the observer design, through the boundary layer design, the saturation function is introduced to replace the traditional signum function to eliminate the chattering of the output of the observer. (*iii*) The variable exponential power reaching law can adapt to the variation of the sliding variable $\boldsymbol{s}$ and can be adjusted adaptively, so as to ensure a fast convergence rate in the whole process.

5. Analysis and calculation of control parameters on the effect of system robustness

By optimizing the constrained QP problem (29), the optimal input control increment $\triangle\ \bar{\boldsymbol{u}}_k$ can be obtained, and then optimal input $\bar{\boldsymbol{u}}_k$ can be solved. Therefore, at time instance k, the velocity acting on the robot motor after compensation by the output of AVPSMO (41) can be calculated as

$$\begin{bmatrix} w_1(k) \\ w_2(k) \\ w_3(k) \\ w_4(k) \end{bmatrix} = \begin{bmatrix} w_1(k-1) \\ w_2(k-1) \\ w_3(k-1) \\ w_4(k-1) \end{bmatrix} + T\boldsymbol{M}^{-1} \begin{bmatrix} u_1(k) \\ u_2(k) \\ u_3(k) \\ u_4(k) \end{bmatrix} - \boldsymbol{J}_{\mathrm{v}} \begin{bmatrix} \hat{f}_{\mathrm{x}}(k) \\ \hat{f}_{\mathrm{y}}(k) \\ \hat{f}_{\omega}(k) \end{bmatrix} \tag{45}$$

where

$$\boldsymbol{J}_{\mathrm{v}} = \frac{1}{r} \begin{bmatrix} 1 & -1 & -(l+L) \\ 1 & 1 & (l+L) \\ 1 & 1 & -(l+L) \\ 1 & -1 & (l+L) \end{bmatrix} \tag{46}$$

is the generalized inverse matrix of $\boldsymbol{J}_{\mathrm{r}}$. Then, at the kth time instance, the kinematic model with disturbances and uncertainties can be written as:

$$\begin{bmatrix} \dot{x}(k) \\ \dot{y}(k) \\ \dot{\varphi}(k) \end{bmatrix} = \boldsymbol{D}_{\mathrm{k}} \left(\boldsymbol{J}_{\mathrm{r}} \begin{bmatrix} w_1(k) \\ w_2(k) \\ w_3(k) \\ w_4(k) \end{bmatrix} + \begin{bmatrix} f_{\mathrm{x}}(k) \\ f_{\mathrm{y}}(k) \\ f_{\omega}(k) \end{bmatrix} \right) \tag{47}$$

where

$$\boldsymbol{D}_{\mathrm{k}} = \begin{bmatrix} \cos[\varphi(k)] & -\sin[\varphi(k)] & 0 \\ \sin[\varphi(k)] & \cos[\varphi(k)] & 0 \\ 0 & 0 & 1 \end{bmatrix}. \tag{48}$$

Substituting Eq. (45) into Eq. (47) yields

$$\begin{bmatrix} \dot{x}(k) \\ \dot{y}(k) \\ \dot{\varphi}(k) \end{bmatrix} = \boldsymbol{D}_{\mathrm{k}} \left(\begin{bmatrix} v_{\mathrm{x}}(k) \\ v_{\mathrm{y}}(k) \\ \omega(k) \end{bmatrix} + \begin{bmatrix} \tilde{f}_{\mathrm{x}}(k) \\ \tilde{f}_{\mathrm{y}}(k) \\ \tilde{f}_{\omega}(k) \end{bmatrix} \right), \tag{49}$$

where

$$\begin{bmatrix} \tilde{f}_{\mathrm{x}}(k) \\ \tilde{f}_{\mathrm{y}}(k) \\ \tilde{f}_{\omega}(k) \end{bmatrix} = \begin{bmatrix} f_{\mathrm{x}}(k) \\ f_{\mathrm{y}}(k) \\ f_{\omega}(k) \end{bmatrix} - \begin{bmatrix} \hat{f}_{\mathrm{x}}(k) \\ \hat{f}_{\mathrm{y}}(k) \\ \hat{f}_{\omega}(k) \end{bmatrix} \tag{50}$$

are the estimated errors of lumped disturbances.

Remark 4. In accordance with *Assumption* 1, notwithstanding the temporal variability in lumped disturbances, the designed AVPSMO (41) can accurately estimate the value of $\boldsymbol{f}$ under the condition that $|d_{i\mathrm{dis}}| < \bar{k}_{2i}, i = 1, 2, 3$, thereby ensuring the robustness of the system. Therefore, it can be proved that the proposed AVPSMO-MPC algorithm in this paper can effectively eliminate the influence of lumped disturbances $\boldsymbol{f}$ and achieve fast and stable tracking control.

The AVPSMO-MPC principle of an MWMR is shown in Fig. 2. The proposed control method is implemented as follows: (1) The nominal dynamics model (14) and the actual kinematics model considering lumped disturbances (17) of the robot are established, respectively. (2) Based on the nominal dynamics model, the model Predictive controller is designed and transformed into a constrained QP problem (29). (3) The constrained QP problem (29) is solved to obtain the optimal control input of the robot. (4) Based on the AVPSMO (41), the lumped disturbances are estimated. (5) According to the estimates in Step 4, the velocities acting on the motor of the follower robot are compensated using Eq. (45). (6) The position information of the reference and follower robots is updated, and the tracking error is calculated. (7) Moving to the next time step and returning the current state value.

6. Simulation results

In this section, to demonstrate the performance of the proposed AVPSMO-MPC algorithm with disturbances and uncertainties considered, two comparative simulation cases are performed based on Matlab. In both simulation cases, the parameters of follower robot R and virtual reference robot R_{r} are the same. The parameters are set to: $r = 0.05$ m, $L = 0.35$ m, $l = 0.25$ m. The total control time T_{c} of the system is 160 s and the sampling time T is 0.1 s.

6.1. Tracking rectangular reference trajectory

In the first simulation case, the proposed AVPSMO-MPC method in this paper and the traditional MPC algorithm are respectively used to control the robot to track a rectangular reference trajectory under the same situation. The parameters of the model predictive controller are chosen as: $N_{\mathrm{p}} = 5$, $N_{\mathrm{c}} = 2$, $\boldsymbol{Q} = \mathrm{diag}(100, 100, 100, 50, 50, 50)$, $\boldsymbol{P} = \mathrm{diag}(1, 1, 1, 1, 1, 1)$. The parameters of AVPSMO (41) are set to: $\varepsilon_1 = \varepsilon_2 = \varepsilon_3 = 0.2, \varsigma_1 = \varsigma_2 = \varsigma_3 = 0.1, \kappa_1 = \kappa_2 = \kappa_3 = 0.2, \sigma_1 = \sigma_2 = \sigma_3 = 0.1$, $\eta_1 = 1.3, \eta_2 = 0.3, \eta_3 = 1.6, \chi = 1$. The lumped disturbances are set to $\boldsymbol{f} = [0.08\sin(0.2t) + 0.04\cos(0.1t), 0.08\cos(0.1t), 0.04\sin(0.2t)]^{\mathrm{T}}$. Moreover, consider the following constraints:

$$\begin{aligned} &[-6, -6, -6, -6]^{\mathrm{T}} \le \boldsymbol{u}_k \le [6, 6, 6, 6]^{\mathrm{T}}, \\ &[-0.5, -0.5, -0.5, -0.5]^{\mathrm{T}} \le \triangle\ \boldsymbol{u}_k \le [0.5, 0.5, 0.5, 0.5]^{\mathrm{T}}. \end{aligned} \tag{51}$$

The angular velocities of four wheels of the virtual robot are given as:

$$\begin{cases} 0 \le T_{\mathrm{c}} \le 40, \\ w_{1\mathrm{r}} = 2\ \mathrm{rad/s}, \\ w_{2\mathrm{r}} = 2\ \mathrm{rad/s}, \\ w_{3\mathrm{r}} = 2\ \mathrm{rad/s}, \\ w_{4\mathrm{r}} = 2\ \mathrm{rad/s}, \end{cases} \begin{cases} 40 < T_{\mathrm{c}} \le 80, \\ w_{1\mathrm{r}} = 2\ \mathrm{rad/s}, \\ w_{2\mathrm{r}} = -2\ \mathrm{rad/s}, \\ w_{3\mathrm{r}} = -2\ \mathrm{rad/s}, \\ w_{4\mathrm{r}} = 2\ \mathrm{rad/s}, \end{cases} \begin{cases} 80 < T_{\mathrm{c}} \le 120, \\ w_{1\mathrm{r}} = -2\ \mathrm{rad/s}, \\ w_{2\mathrm{r}} = -2\ \mathrm{rad/s}, \\ w_{3\mathrm{r}} = -2\ \mathrm{rad/s}, \\ w_{4\mathrm{r}} = -2\ \mathrm{rad/s}, \end{cases} \begin{cases} 120 < T_{\mathrm{c}} \le 160, \\ w_{1\mathrm{r}} = -2\ \mathrm{rad/s}, \\ w_{2\mathrm{r}} = 2\ \mathrm{rad/s}, \\ w_{3\mathrm{r}} = 2\ \mathrm{rad/s}, \\ w_{4\mathrm{r}} = -2\ \mathrm{rad/s}. \end{cases} \tag{52}$$

The initial positions and orientation angles of robots R_{r} and R are set to $(x_{\mathrm{r}}, y_{\mathrm{r}}, \varphi_{\mathrm{r}}) = (5\ \mathrm{m}, 3\ \mathrm{m}, 0\ \mathrm{rad})$ and $(x, y, \varphi) = (4\ \mathrm{m}, 3.2\ \mathrm{m}, 0\ \mathrm{rad})$, respectively. The trajectories are shown in Fig. 3. From Fig. 3 and its partial enlarged figure, it is easy to find that the AVPSMO-MPC algorithm can make robot follow the reference trajectory completely. However, the trajectory exhibits a certain error with respect to the reference trajectory when only the MPC method is used. It is shown that the AVPSMO-MPC method can eliminate the influence of disturbances and improve the accuracy of trajectory tracking. The tracking errors of the system are shown in Fig. 4. It is evident that all the errors fully converge to zero when the AVPSMO-MPC method is used, whereas certain errors persist when the traditional MPC method is used.

Fig. 5 shows the estimations of the lumped disturbances. Although the lumped disturbances change irregularly, the designed AVPSMO can still estimate the disturbance value quickly and accurately with almost no estimation error or chattering. The actual angular velocities between the wheels and the ground can be defined as $[\bar{w}_1, \bar{w}_2, \bar{w}_3, \bar{w}_4]^{\mathrm{T}}$. Combining Eq. (45) to Eq. (50), yields

$$\begin{bmatrix} \bar{w}_1(k) \\ \bar{w}_2(k) \\ \bar{w}_3(k) \\ \bar{w}_4(k) \end{bmatrix} = \begin{bmatrix} w_1(k) \\ w_2(k) \\ w_3(k) \\ w_4(k) \end{bmatrix} + \boldsymbol{J}_{\mathrm{v}} \begin{bmatrix} f_{\mathrm{x}}(k) \\ f_{\mathrm{y}}(k) \\ f_{\omega}(k) \end{bmatrix}. \tag{53}$$

The coupling constraint relationship between the angular velocities of the four wheels [18] is shown in Fig. 6. It can be found that the coupling constraint of the velocity is always maintained during the entire tracking process. The actual angular velocities of the four wheels are shown in Figs. 7–10. When the AVPSMO-MPC method is used, the velocities of the four wheels can fully converge to the desired velocities; however, the effect of the MPC method is not ideal.

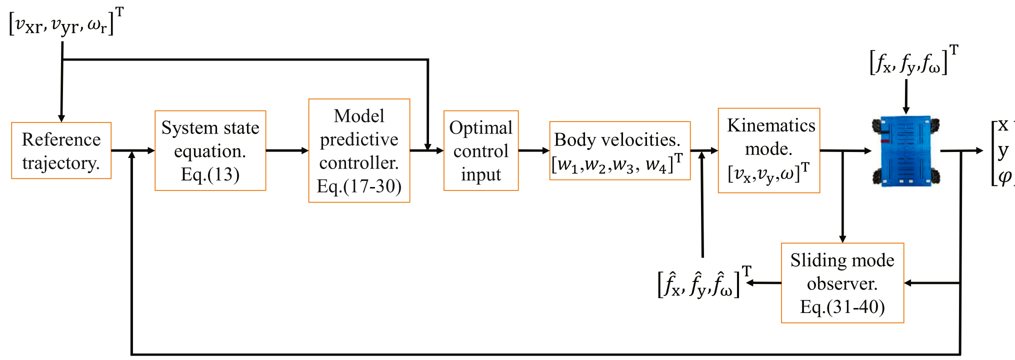

Fig. 2. Block diagram of the proposed AVPSMO-MPC algorithm.

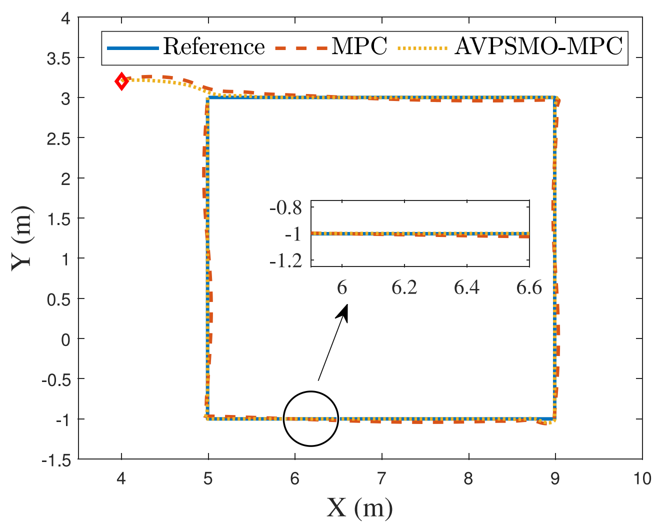

Fig. 3. Trajectory tracking result of rectangular trajectory.

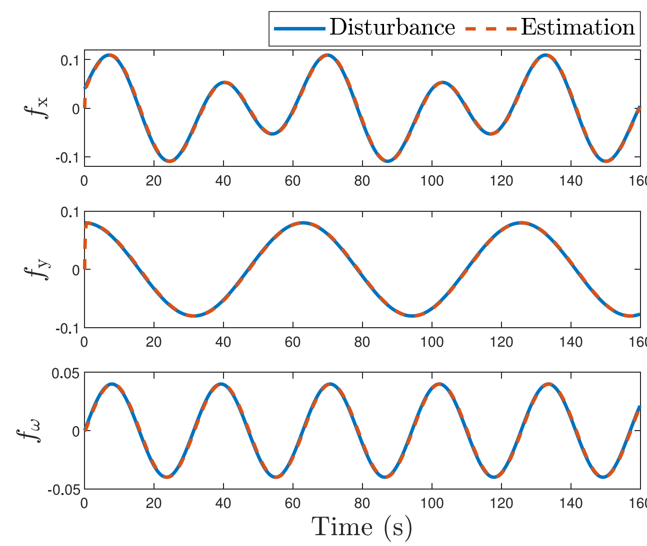

Fig. 5. Estimations of lumped disturbances.

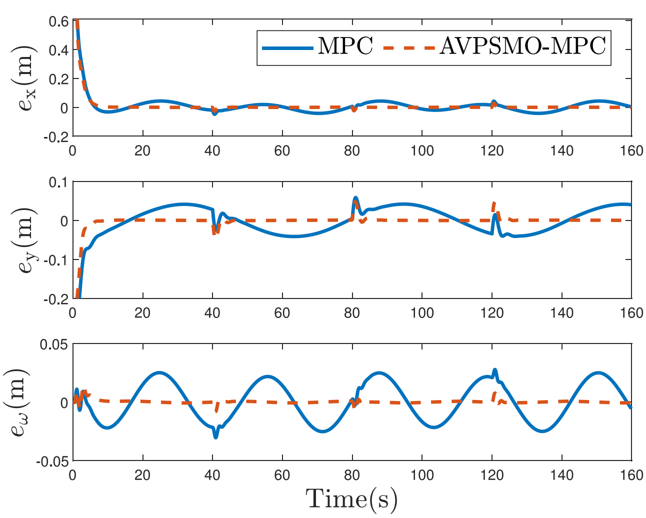

Fig. 4. Comparison of rectangular trajectory tracking errors.

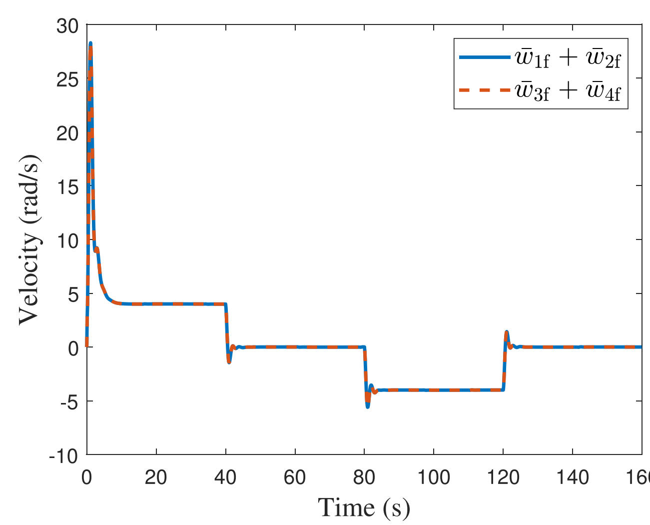

Fig. 6. The velocity constraint verification.

6.2. Tracking S-shaped reference trajectory

In the second simulation case, 30 times independent repeated simulation experiments are conducted, where the follower is tasked with tracking a reference robot from various initial setpoints. Moreover, in order to verify the disturbance rejection ability of the proposed method, the disturbance values are different in each simulation experiment. Comparative analysis with latest high-impact methods [39,42,44,45] are illustrated to prove the superiority of the proposed AVPSMO-MPC. The methods in literature [39,42,44,45] can be expressed as follows:

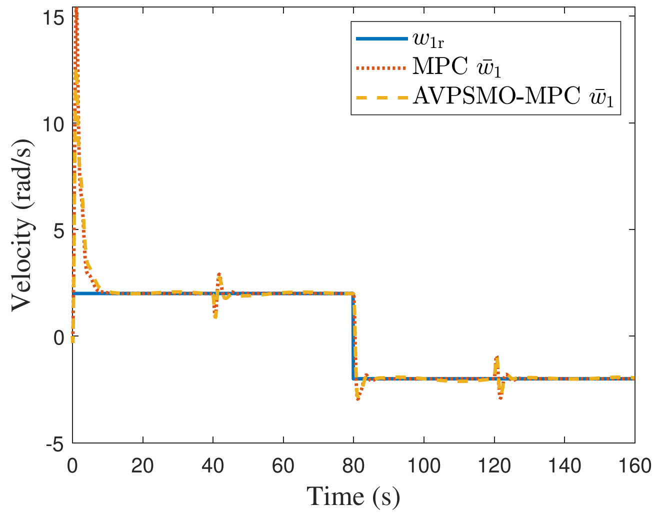

Fig. 7. Angular velocity versus time plot of wheel 1.

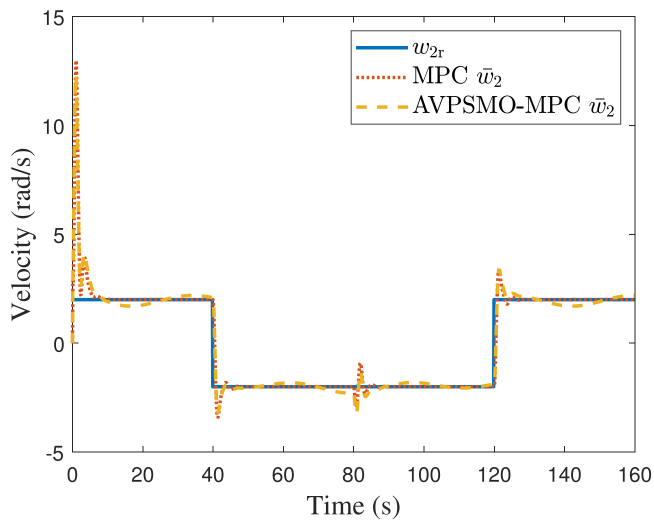

Fig. 8. Angular velocity versus time plot of wheel 2.

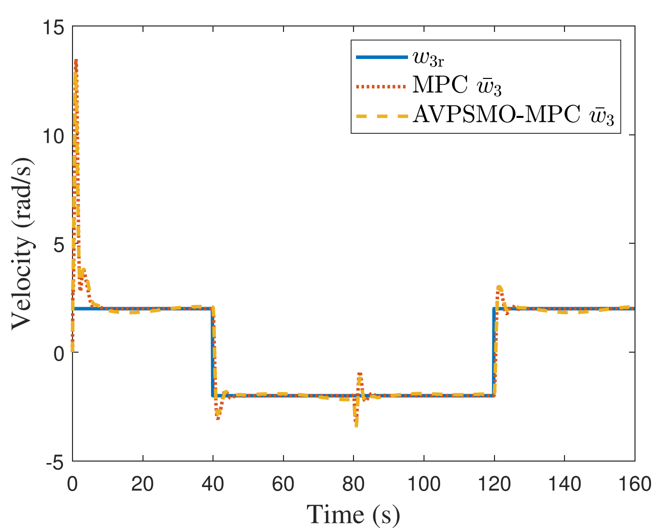

Fig. 9. Angular velocity versus time plot of wheel 3.

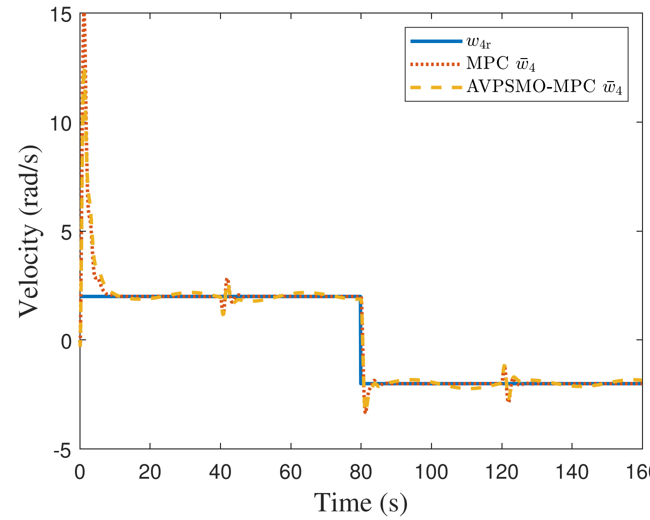

Fig. 10. Angular velocity versus time plot of wheel 4.

• The double power sliding mode observer (DPSMO) in [39]: The double power reaching law is given as $\dot{\boldsymbol{s}} = -\boldsymbol{K}_1\boldsymbol{s} - \boldsymbol{K}_2\mathbf{sat}(\boldsymbol{s}) - \boldsymbol{K}_3|\boldsymbol{s}|^{\varepsilon_1\boldsymbol{E}}\mathbf{sat}(\boldsymbol{s}) - \boldsymbol{K}_4|\boldsymbol{s}|^{\varepsilon_2\boldsymbol{E}}\mathbf{sat}(\boldsymbol{s})$. Then, the observer can be designed as $\dot{\hat{\boldsymbol{z}}} = \bar{\boldsymbol{B}}\boldsymbol{v} + \boldsymbol{K}_1\boldsymbol{s} + \boldsymbol{K}_2\mathbf{sat}(\boldsymbol{s}) + \boldsymbol{K}_3|\boldsymbol{s}|^{\varepsilon_1\boldsymbol{E}}\mathbf{sat}(\boldsymbol{s}) + \boldsymbol{K}_4|\boldsymbol{s}|^{\varepsilon_2\boldsymbol{E}}\mathbf{sat}(\boldsymbol{s})$, where $0 < \varepsilon_1 < 1$, $\varepsilon_2 > 1$ and the definition of other parameters are consistent with those described in Eq. (36).

• The sliding mode disturbance observer (SMDO) in [42]: The reaching law is given as $\dot{\boldsymbol{s}} = -\boldsymbol{K}_1\boldsymbol{s} - \boldsymbol{K}_2\mathbf{sat}(\boldsymbol{s})$. Then, the observer can be designed as $\dot{\hat{\boldsymbol{z}}} = \bar{\boldsymbol{B}}\boldsymbol{v} + \boldsymbol{K}_1\boldsymbol{s} + \boldsymbol{K}_2\mathbf{sat}(\boldsymbol{s})$, where $\boldsymbol{K}_1$ and $\boldsymbol{K}_2$ are positive definite.

• The adaptive terminal sliding mode disturbance observer (ATSMDO) in [44]: The sliding surface is given as $\boldsymbol{s} = \boldsymbol{e} + \boldsymbol{K}_1\dot{\boldsymbol{e}} + \boldsymbol{K}_2\dot{\boldsymbol{e}}^{\frac{m}{n}}$, where $\boldsymbol{e} = \boldsymbol{z} - \hat{\boldsymbol{z}}$. The reaching law is given as $\dot{\boldsymbol{s}} = \boldsymbol{K}_3\boldsymbol{s} + \boldsymbol{K}_4\mathbf{sgn}(\boldsymbol{s})$. Then, the observer can be designed as $\dot{\hat{\boldsymbol{z}}} = \bar{\boldsymbol{B}}\boldsymbol{v} + \hat{\boldsymbol{f}}$, where $\hat{\boldsymbol{f}} = [\boldsymbol{K}_1 + \frac{m}{n}\boldsymbol{K}_2\dot{\boldsymbol{e}}^{\frac{(m-n)}{n}}]^{-1}[\dot{\boldsymbol{e}} + \boldsymbol{K}_3\boldsymbol{s} + \boldsymbol{K}_4\mathbf{sgn}(\boldsymbol{s})] + \dot{\hat{\boldsymbol{\alpha}}}$. $\boldsymbol{K}_1$, $\boldsymbol{K}_2$, $\boldsymbol{K}_3$ and $\boldsymbol{K}_4$ are positive definite, and $2n > m > n > 0$. $\dot{\hat{\boldsymbol{\alpha}}} = \rho[\boldsymbol{K}_1 + \frac{m}{n}\boldsymbol{K}_2\dot{\boldsymbol{e}}^{\frac{(m-n)}{n}}]\boldsymbol{s}$ as an adaptive gain, where ρ is a positive constant. The definition of other parameters are consistent with those described in Eq. (36).

• The new extended state observer (NESO) in [45]: The observer can be designed as $\dot{\hat{\boldsymbol{z}}} = \bar{\boldsymbol{B}}\boldsymbol{v} + \frac{g(\boldsymbol{e})}{\varepsilon}$, where $g(\cdot)$ is a odd continuous function, $\varepsilon < 1$ is a small positive constant.

Define the number of experiments as $n_{\mathrm{e}} = 1, 2, \ldots, 30$, the initial states of robot R_{r} and R are set to $(x_{\mathrm{r}}, y_{\mathrm{r}}, \varphi_{\mathrm{r}}) = (5\ \mathrm{m}, 3\ \mathrm{m}, 0\ \mathrm{rad})$ and $(x, y, \varphi) = ((4-0.01n_{\mathrm{e}})\ \mathrm{m}, (2-0.01n_{\mathrm{e}})\ \mathrm{m}, 0\ \mathrm{rad})$, respectively. The angular velocities of four wheels of the virtual robot are given as:

$$\begin{cases} 0 \le T_{\mathrm{c}} \le 80, \\ w_{1\mathrm{r}} = 1.2\ \mathrm{rad/s}, \\ w_{2\mathrm{r}} = 1.3\ \mathrm{rad/s}, \\ w_{3\mathrm{r}} = 1\ \mathrm{rad/s}, \\ w_{4\mathrm{r}} = 1.5\ \mathrm{rad/s}, \end{cases} \quad \begin{cases} 80 < T_{\mathrm{c}} \le 160, \\ w_{1\mathrm{r}} = 1.5\ \mathrm{rad/s}, \\ w_{2\mathrm{r}} = 1\ \mathrm{rad/s}, \\ w_{3\mathrm{r}} = 1.3\ \mathrm{rad/s}, \\ w_{4\mathrm{r}} = 1.2\ \mathrm{rad/s}, \end{cases} \tag{54}$$

The parameter settings of MPC are the same as in the first simulation case. The parameter settings of the observers are as follows:

• DPSMO: $\boldsymbol{K}_1 = 3\boldsymbol{E}, \boldsymbol{K}_2 = \boldsymbol{E},\ \boldsymbol{K}_3 = 3\boldsymbol{E}, \boldsymbol{K}_4 = \boldsymbol{E},\ \varepsilon_1 = 1.5,\ \varepsilon_2 = 0.5$;

• SMDO: $\boldsymbol{K}_1 = 3\boldsymbol{E},\ \boldsymbol{K}_2 = \boldsymbol{E}$;

• ATSMDO: $\boldsymbol{K}_1 = \boldsymbol{E}, \boldsymbol{K}_2 = 0.1\boldsymbol{E},\ \boldsymbol{K}_3 = 3\boldsymbol{E}, \boldsymbol{K}_4 = 0.05\boldsymbol{E},\ m = 2,\ n = 1,$ $\rho = 0.07$;

• NESO: $g(\boldsymbol{e}) = \boldsymbol{e},\ \varepsilon = 0.1$;

• AVPSMO: $\varepsilon_1 = \varepsilon_2 = \varepsilon_3 = 0.2, \varsigma_1 = \varsigma_2 = \varsigma_3 = 0.2, \kappa_1 = \kappa_2 = \kappa_3 = 0.2, \sigma_1 = \sigma_2 = \sigma_3 = 0.1,\ \eta_1 = 1.5, \eta_2 = 0.1$ and $\eta_3 = 1.5$.

Under the above parameter settings, thirty times tracking experiments are performed using DPSMO-MPC, SMDO-MPC, ATSMDO-MPC, NESO-MPC and AVPSMO-MPC, respectively. In the n_eth experiment,

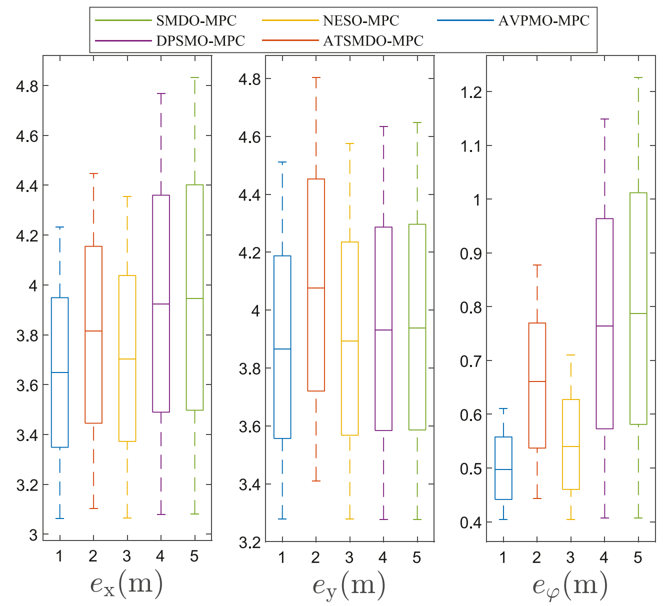

Fig. 11. Comparisons of the integral absolute tracking errors from 30 tracking experiments.

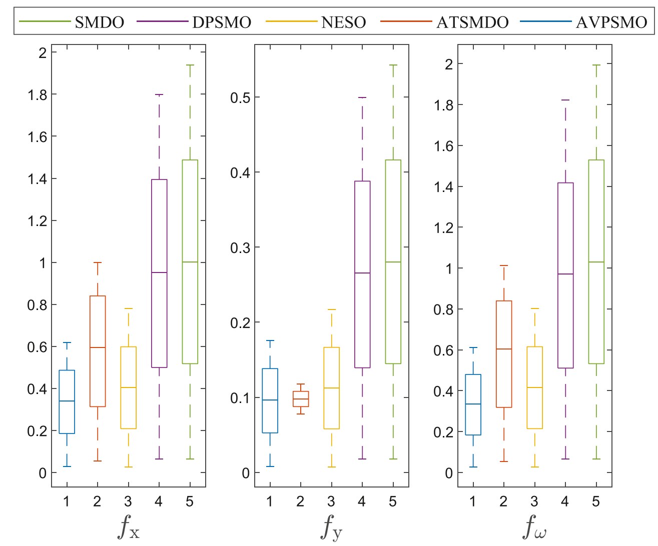

Fig. 12. Comparisons of the integral absolute disturbance estimation errors from 30 tracking experiments.

the lumped disturbances are set to: $\boldsymbol{f} = 0.01n_e[f_x, f_y, f_\omega]^T$, where $f_x = 0.5 + 0.5\sin(0.5t)$, $f_y = \sin(0.07t) + 0.5\cos(0.05t)$ and $f_\omega = \sin(0.1t) + 0.5\cos(0.5t)$.

To evaluate the tracking performance of DPSMO-MPC, SMDO-MPC, ATSMDO-MPC, NESO-MPC and AVPSMO-MPC, the integral absolute tracking errors (IAE) and integral absolute disturbance estimation errors from 30 tracking experiments are shown as boxplots in Fig. 11 and Fig. 12, respectively. These boxplots intuitively demonstrate that the IAE corresponding to the proposed AVPSMO-MPC method is smaller and more centralized than those of the other algorithms. Notably, Fig. 11 signifies that the proposed strategy has a better tracking performance, and Fig. 12 substantiates that the proposed AVPSMO-MPC can more accurately estimate disturbances, thereby demonstrating the robustness of the algorithm. It is evident that the proposed algorithm excels in disturbance suppression and exhibits excellent tracking performance for various setpoints.

In addition, we record the results of one of the comparative simulation cases in detail. The tracking results and the integral absolute tracking errors for the S-shaped trajectory with above five controllers are shown in Fig. 13 and Fig. 14, respectively. Although each of the five control algorithms have good control effect, the AVPSMO-MPC method proposed in this paper has a smaller tracking error. The estimated disturbance values and the integral absolute disturbance estimation errors are shown in Fig. 15 and Fig. 16, respectively. In the 30 simulation cases, the AVPSMO is generally able to converge within 2s. Moreover, as shown in Figs. 15–16, AVPSMO-MPC has superior accuracy in terms of disturbance estimation compared with other algorithms.

From the above comparative simulation cases, the following conclusions can be made:

(1) Compared with the traditional MPC method, the proposed AVPSMO-MPC strategy can realize more stable tracking control in the presence of disturbances and uncertainties, and can ensure that various constraints are not violated;
(2) The AVPSMO designed in this paper can quickly and accurately approximate unknown lumped disturbances. Moreover, the effect of chattering is almost completely eliminated;
(3) In repeated simulation experiments, each experiment is independent with different setpoints and disturbances. The proposed AVPSMO-MPC consistently demonstrates its ability to effectively suppress disturbances and achieve precise and stable tracking in the aforementioned situations.

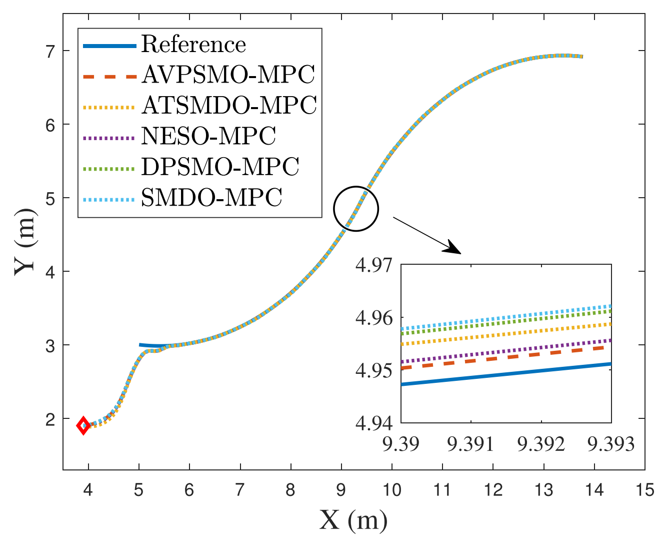

Fig. 13. Trajectory tracking result of S-shaped trajectory.

7. Conclusion

Aiming at the tracking control problem of the MWMR under the influence of unknown disturbances and model uncertainties, an AVPSMO-MPC algorithm is proposed in this paper. First, considering various physical constraints, the unmeasurable lumped disturbance is incorporated into the nominal model, and a control problem with trajectory tracking and disturbance rejection is established. To eliminate the effect of model error caused by external disturbances and uncertainties, an AVPSMO is introduced to approximate the disturbance online. The proposed observer can adaptively adjust the reaching law parameter based on observation errors. The stability and robustness of the designed sliding mode observer are rigorously proven. On this basis, a model predictive controller is designed for the tracking control of the

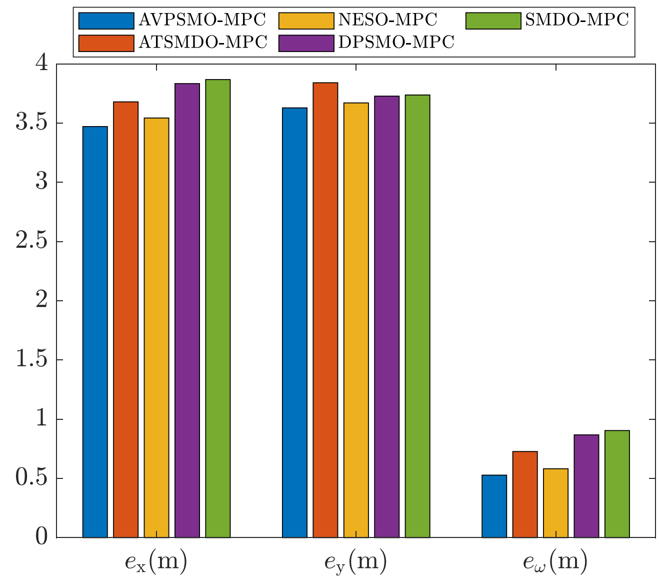

Fig. 14. Comparisons of the integral absolute tracking errors.

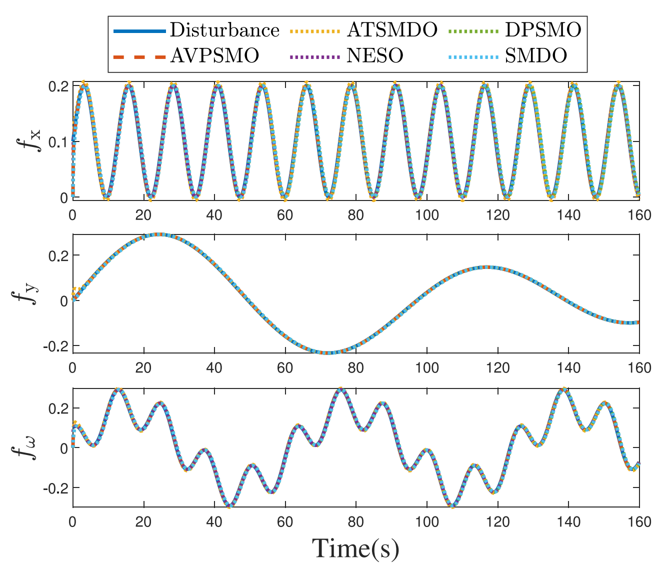

Fig. 15. Estimations of lumped disturbances.

MWMR. Finally, the effectiveness and robustness of the proposed control algorithm is verified by comparative simulation cases. Simulation results indicate that the proposed AVPSMO-MPC method effectively suppresses tracking errors caused by the lumped disturbances, improves the performance of tracking control, with faster response compared with other methods.

Future research may focus on predictive control for more different application scenarios. For example, learning predictive control theory and method for time-delay systems, and communication constrained and event triggered distributed learning control.

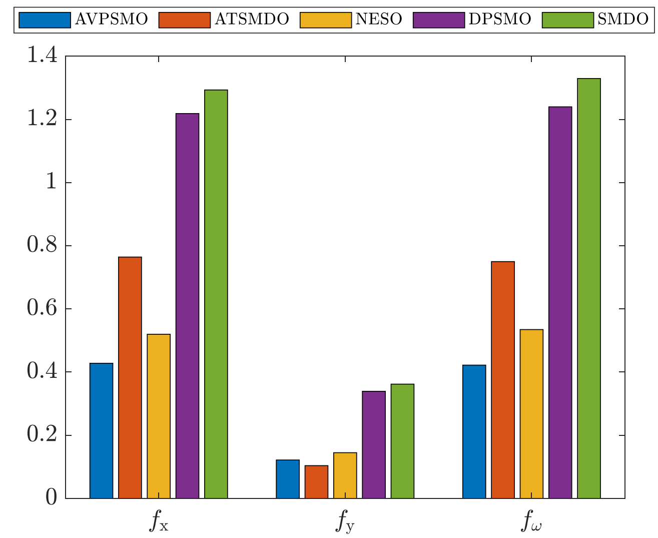

Fig. 16. Comparisons of the integral absolute disturbance estimation errors.

CRediT authorship contribution statement

Dongliang Wang: Writing – review & editing, Writing – original draft, Visualization, Methodology, Conceptualization. **Yong Gao:** Writing – review & editing, Visualization. **Wu Wei:** Supervision, Funding acquisition. **Qiuda Yu:** Methodology, Investigation. **Yuhai Wei:** Investigation, Data curation. **Wenji Li:** Validation, Data curation. **Zhun Fan:** Supervision, Investigation.

Acknowledgments

This research is funded by the Science and Technology Planning Project of Guangdong Province, China (grant numbers 2022A1515110566, 2023A1515011574, 2019A050520001), the STU Scientific Research Initiation Grant NTF21052.

Declaration of competing interest

The authors declare that they have no known competing financial interests or personal relationships that could have appeared to influence the work reported in this paper.

References

[1] Huang HC, Lin SK. A hybrid metaheuristic embedded system for intelligent vehicles using hypermutated firefly algorithm optimized radial basis function neural network. IEEE Trans Ind Inf 2018;15(2):1062–9. http://dx.doi.org/10.1109/TII.2018.2796556.

[2] Rauniyar A, Upreti HC, Mishra A, Sethuramalingam P. MeWbots: Mecanum-wheeled robots for collaborative manipulation in an obstacle-clustered environment without communication. J Intell Robot Syst 2021;102:1–18. http://dx.doi.org/10.1007/s10846-021-01359-5.

[3] Hou L, Zhou F, Kim K, Zhang L. Practical model for energy consumption analysis of omnidirectional mobile robot. Sensors 2021;21(5):1800. http://dx.doi.org/10.3390/s21051800.

[4] Siegwart R, Nourbakhsh IR, Scaramuzza D. Introduction to autonomous mobile robots. MIT Press; 2011.

[5] Zhao T, Zou X, Dian S. Fixed-time observer-based adaptive fuzzy tracking control for Mecanum-wheel mobile robots with guaranteed transient performance. Nonlinear Dynam 2022;1–17. http://dx.doi.org/10.1007/s11071-021-06985-0.

[6] Mellah S, Graton G, El Adel EM, Ouladsine M, Planchais A. Health state monitoring of 4-Mecanum wheeled mobile robot actuators and its impact on the robot behavior analysis. J Intell Robot Syst 2021;102(4):86. http://dx.doi.org/10.1007/s10846-021-01446-7.

[7] Serrano ME, Gandolfo DC, Scaglia GJ. Trajectory tracking controller for unmanned helicopter under environmental disturbances. ISA Trans 2020;106:171–80. http://dx.doi.org/10.1016/j.isatra.2020.06.026.

[8] Jing C, Xu H, Niu X. Adaptive sliding mode disturbance rejection control with prescribed performance for robotic manipulators. ISA Trans 2019;91:41–51. http://dx.doi.org/10.1016/j.isatra.2019.01.017.

[9] Yuan Z, Tian Y, Yin Y, Wang S, Liu J, Wu L. Trajectory tracking control of a four Mecanum wheeled mobile platform: An extended state observer-based sliding mode approach. IET Control Theory Appl 2020;14(3):415–26. http://dx.doi.org/10.1049/iet-cta.2018.6127.

[10] Sun Z, Hu S, He D, Zhu W, Xie H, Zheng J. Trajectory-tracking control of Mecanum-wheeled omnidirectional mobile robots using adaptive integral terminal sliding mode. Comput Electr Eng 2021;96:107500. http://dx.doi.org/10.1016/j.compeleceng.2021.107500.
[11] Cao G, Zhao X, Ye C, Yu S, Li B, Jiang C. Fuzzy adaptive PID control method for multi-Mecanum-wheeled mobile robot. J Mech Sci Technol 2022;36(4):2019–29. http://dx.doi.org/10.1007/s12206-022-0337-x.
[12] Wang D, Wei W, Wang X, Gao Y, Li Y, Yu Q, et al. Formation control of multiple Mecanum-wheeled mobile robots with physical constraints and uncertainties. Appl Intell 2022;1–20. http://dx.doi.org/10.1007/s10489-021-02459-3.
[13] Zarei J, Masoudi E, Razavi-Far R, Saif M. Fault-tolerant control design for unreliable networked control systems via constrained model predictive control. ISA Trans 2023;134:171–82. http://dx.doi.org/10.1016/j.isatra.2022.08.019.
[14] Gao Y, Wei W, Wang X, Wang D, Li Y, Yu Q. Trajectory tracking of multi-legged robot based on model predictive and sliding mode control. Inform Sci 2022;606:489–511. http://dx.doi.org/10.1016/j.ins.2022.05.069.
[15] Li Z, Wang P, Cai S, Hu X, Chen H. NMPC-based controller for vehicle longitudinal and lateral stability enhancement under extreme driving conditions. ISA Trans 2023;135:509–23. http://dx.doi.org/10.1016/j.isatra.2022.09.038.
[16] Karras GC, Fourlas GK. Model predictive fault tolerant control for omni-directional mobile robots. J Intell Robot Syst 2020;97:635–55. http://dx.doi.org/10.1007/s10846-019-01029-7.
[17] Lafmejani AS, Berman S, Fainekos G. NMPC-LBF: Nonlinear MPC with learned barrier function for decentralized safe navigation of multiple robots in unknown environments. In: 2022 IEEE/RSJ international conference on intelligent robots and systems. 2022, p. 10297–303. http://dx.doi.org/10.1109/IROS47612.2022.9981177.
[18] Wang D, Wei W, Yeboah Y, Li Y, Gao Y. A robust model predictive control strategy for trajectory tracking of omni-directional mobile robots. J Intell Robot Syst 2020;98:439–53. http://dx.doi.org/10.1007/s10846-019-01083-1.
[19] Yu J, Zhu Z, Lu J, Yin S, Zhang Y. Modeling and MPC-Based pose tracking for wheeled bipedal robot. IEEE Robot Autom Lett 2023;8(12):7881–8. http://dx.doi.org/10.1109/LRA.2023.3322084.
[20] Xiao H, Yu D, Chen CP. Self-triggered-organized mecanum-wheeled robots consensus system using model predictive based protocol. Inform Sci 2022;590:45–59. http://dx.doi.org/10.1016/j.ins.2021.12.108.
[21] Yang R, Zheng L, Pan J, Cheng H. Learning-based predictive path following control for nonlinear systems under uncertain disturbances. IEEE Robot. Autom. Lett. 2021;6(2):2854–61. http://dx.doi.org/10.1109/LRA.2021.3062805.
[22] Zhang B, Sun X, Liu S, Deng X. Adaptive model predictive control with extended state observer for multi-UAV formation flight. Internat J Adapt Control Signal Process 2020;34(10):1341–58. http://dx.doi.org/10.1002/acs.3145.
[23] Yang J, Li S, Yu X. Sliding-mode control for systems with mismatched uncertainties via a disturbance observer. IEEE Trans Ind Electron 2012;60(1):160–9. http://dx.doi.org/10.1109/TIE.2012.2183841.
[24] Zhang J, Feng G, Xia Y. Design of estimator-based sliding-mode output-feedback controllers for discrete-time systems. IEEE Trans Ind Electron 2013;61(5):2432–40. http://dx.doi.org/10.1109/TIE.2013.2274413.
[25] Zhang H, Zhou X, Wang Z, Yan H, Sun J. Adaptive consensus-based distributed target tracking with dynamic cluster in sensor networks. IEEE Trans Cybern 2018;49(5):1580–91. http://dx.doi.org/10.1109/TCYB.2018.2805717.
[26] Kang HS, Kim YT, Hyun CH, Park M. Generalized extended state observer approach to robust tracking control for wheeled mobile robot with skidding and slipping. Int J Adv Robot Syst 2013;10(3):155. http://dx.doi.org/10.5772/55738.
[27] Peng Z, Wang J. Output-feedback path-following control of autonomous underwater vehicles based on an extended state observer and projection neural networks. IEEE Trans Syst, Man, Cybern -Syst 2017;48(4):535–44. http://dx.doi.org/10.1109/TSMC.2017.2697447.
[28] Alakshendra V, Chiddarwar SS. Adaptive robust control of mecanum-wheeled mobile robot with uncertainties. Nonlinear Dynam 2017;87:2147–69. http://dx.doi.org/10.1007/s11071-016-3179-1.
[29] Liu A, Zhang WA, Yu L, Yan H, Zhang R. Formation control of multiple mobile robots incorporating an extended state observer and distributed model predictive approach. IEEE Trans Syst Man Cybern -Syst 2018;50(11):4587–97. http://dx.doi.org/10.1109/TSMC.2018.2855444.
[30] Qiao Z, Shi T, Wang Y, Yan Y, Xia C, He X. New sliding-mode observer for position sensorless control of permanent-magnet synchronous motor. IEEE Trans Ind Electron 2012;60(2):710–9. http://dx.doi.org/10.1109/TIE.2012.2206359.
[31] Sun T, Cheng L, Hou Z, Tan M. Novel sliding-mode disturbance observer-based tracking control with applications to robot manipulators. Sci China-Inf Sci 2021;64(7):172205. http://dx.doi.org/10.1007/s11432-020-3043-y.
[32] Sun X, Cao J, Lei G, Guo Y, Zhu J. A robust deadbeat predictive controller with delay compensation based on composite sliding-mode observer for PMSMs. IEEE Trans Power Electron 2021;36(9):10742–52. http://dx.doi.org/10.1109/TPEL.2021.3063226.
[33] Sun T, Cheng L, Wang W, Pan Y. Semiglobal exponential control of Euler–Lagrange systems using a sliding-mode disturbance observer. Automatica 2020;112:108677. http://dx.doi.org/10.1016/j.automatica.2019.108677.
[34] Rafiq M, Rehman SU, Rehman FU, Butt QR, Awan I. A second order sliding mode control design of a switched reluctance motor using super twisting algorithm. Simul Model Pract Theory 2012;25:106–17. http://dx.doi.org/10.1016/j.simpat.2012.03.001.
[35] Gao Y, Wei W, Wang X, Li Y, Wang D, Yu Q. Feasibility, planning and control of ground-wall transition for a suctorial hexapod robot. Appl Intell 2021;1–19. http://dx.doi.org/10.1007/s10489-020-01955-2.
[36] Xiong X, Kikuuwe R, Kamal S, Jin S. Implicit-Euler implementation of super-twisting observer and twisting controller for second-order systems. IEEE Trans Circuits Syst II-Express Briefs 2019;67(11):2607–11. http://dx.doi.org/10.1109/TCSII.2019.2957271.
[37] Van M, Kang HJ, Suh YS. A novel fuzzy second-order sliding mode observer-controller for a TS fuzzy system with an application for robot control. Int J Precis Eng Manuf 2013;14:1703–11. http://dx.doi.org/10.1007/s12541-013-0229-1.
[38] Zhao K, Leng A, Zhou R, Dai W, Wu S, Li T. Demagnetization fault reconstruction for six-phase permanent magnet synchronous motor by improved super-twisting algorithm-based sliding-mode observer. Measurement 2021;172:108905. http://dx.doi.org/10.1016/j.measurement.2020.108905.
[39] Pan J, Li W, Zhang H. Control algorithms of magnetic suspension systems based on the improved double exponential reaching law of sliding mode control. Int J Control Autom Syst 2018;16(6):2878–87. http://dx.doi.org/10.1007/s12555-017-0616-y.
[40] Kim H, Son J, Lee J. A high-speed sliding-mode observer for the sensorless speed control of a PMSM. IEEE Trans Ind Electron 2010;58(9):4069–77. http://dx.doi.org/10.1109/TIE.2010.2098357.
[41] Cui M, Liu W, Liu H, Jiang H, Wang Z. Extended state observer-based adaptive sliding mode control of differential-driving mobile robot with uncertainties. Nonlinear Dynam 2016;83:667–83. http://dx.doi.org/10.1007/s11071-015-2355-z.
[42] Deng Y, Wang J, Li H, Liu J, Tian D. Adaptive sliding mode current control with sliding mode disturbance observer for PMSM drives. ISA Trans 2019;88:113–26. http://dx.doi.org/10.1016/j.isatra.2018.11.039.
[43] Tsai CC, Wu HL. Nonsingular terminal sliding control using fuzzy wavelet networks for mecanum wheeled omni-directional vehicles. In: International conference on fuzzy systems. IEEE; 2010, p. 1–6. http://dx.doi.org/10.1109/FUZZY.2010.5584223.
[44] Gurumurthy G, Das DK. Terminal sliding mode disturbance observer based adaptive super twisting sliding mode controller design for a class of nonlinear systems. Eur J Control 2021;57:232–41. http://dx.doi.org/10.1016/j.ejcon.2020.05.004.
[45] Ran M, Li J, Xie L. A new extended state observer for uncertain nonlinear systems. Automatica 2021;131:109772. http://dx.doi.org/10.1016/j.automatica.2021.109772.